

## The use of amorphous boron powder enhances mechanical alloying in soft magnetic FeNbB alloy: A magnetic study

J. J. Ipus, J. S. Blázquez, V. Franco, and A. Conde

Citation: [Journal of Applied Physics](#) **113**, 17A330 (2013); doi: 10.1063/1.4798794

View online: <http://dx.doi.org/10.1063/1.4798794>

View Table of Contents: <http://scitation.aip.org/content/aip/journal/jap/113/17?ver=pdfcov>

Published by the [AIP Publishing](#)

---

### Articles you may be interested in

[Magnetic and magnetoimpedance studies on controlled Joule annealed amorphous Co<sub>73</sub>Fe<sub>4.5</sub>Ni<sub>0.5</sub>Mn<sub>0.5</sub>Nb<sub>0.5</sub>Si<sub>4.2</sub>B<sub>16.8</sub> alloy](#)

[J. Appl. Phys.](#) **115**, 17A324 (2014); 10.1063/1.4865767

[Structure and magnetic properties of Fe–Nb–B amorphous/nanocrystalline alloys produced by compaction of mechanically alloyed powders](#)

[J. Appl. Phys.](#) **107**, 073901 (2010); 10.1063/1.3319669

[Improvement of soft magnetic properties by simultaneous addition of P and Cu for nanocrystalline FeNbB alloys](#)

[J. Appl. Phys.](#) **101**, 09N117 (2007); 10.1063/1.2714676

[Optimization of the microstructure and properties of Co-substituted Fe–Si–B–Nb–Cu nanocrystalline soft magnetic alloys](#)

[J. Appl. Phys.](#) **93**, 9186 (2003); 10.1063/1.1569396

[Soft magnetic properties and structures of nanocrystalline Fe–Al–Si–B–Cu–Nb alloy ribbons](#)

[J. Appl. Phys.](#) **83**, 6335 (1998); 10.1063/1.367836

---


 **SHIMADZU**  
Excellence in Science

**Powerful, Multi-functional UV-Vis-NIR and FTIR Spectrophotometers**

Providing the utmost in sensitivity, accuracy and resolution for applications in materials characterization and nano research

- Photovoltaics
- Polymers
- Thin films
- Paints
- Ceramics
- DNA film structures
- Coatings
- Packaging materials

[Click here to learn more](#)

A row of four Shimadzu spectrophotometers is shown. From left to right: a small benchtop model, a larger benchtop model with a sample holder, a large floor-standing model with a wide sample area, and a large floor-standing model with a complex sample handling system.

# The use of amorphous boron powder enhances mechanical alloying in soft magnetic FeNbB alloy: A magnetic study

J. J. Ipus,<sup>a)</sup> J. S. Blázquez, V. Franco, and A. Conde

*Dpto. Física de la Materia Condensada, ICMSE-CSIC, Universidad de Sevilla, P.O. Box 1065, 41080 Sevilla, Spain*

(Presented 17 January 2013; received 1 November 2012; accepted 4 January 2013; published online 3 April 2013)

Saturation magnetization and magnetic anisotropy have been studied during mechanical alloying of Fe<sub>75</sub>Nb<sub>10</sub>B<sub>15</sub> alloys prepared using crystalline and commercial amorphous boron. The evolution of saturation magnetization indicates a more efficient dissolution of boron into the matrix using amorphous boron, particularly for short milling times. The magnetization of the crystalline phase increases as boron is incorporated into this phase. Two milling time regimes can be used to describe the evolution of magnetic anisotropy: a first regime governed by microstrains and a second one mainly governed by crystal size and amorphous fraction. © 2013 American Institute of Physics. [<http://dx.doi.org/10.1063/1.4798794>]

## I. INTRODUCTION

Amorphous and nanocrystalline Fe-based soft magnetic alloys have deserved the attention of the scientific community since the discovery of Metglas and Finemet<sup>1,2</sup> systems. These two systems, and other similar ones produced by ultra rapid quenching techniques, must include metalloid elements in their compositions, such as B, Si, P, to enhance the glass forming ability. In the case of boron addition to Fe-based amorphous alloys, magnetic properties are also enhanced for boron contents up to ~30 at. %.

Systems produced by rapid quenching techniques are generally limited in shape to wires or ribbons, as one of the requirements for rapid heat transfer is a high surface to volume ratio. In order to overcome this limitation, powder metallurgy is an attractive way to produce these alloys. In fact, mechanical alloying has been shown to be very effective in producing amorphous phases in a wide compositional range, which can overlap with those obtained by rapid quenching.<sup>3</sup> However, properties such as Curie temperature of boron containing alloys produced by ball milling from pure powders indicate that the boron content of such amorphous phases does not correspond to the expected value for the nominal composition.<sup>4,5</sup> Recently, the presence of remaining inclusions of almost pure boron was observed even after long milling times,<sup>4</sup> which must affect the actual composition of the amorphous phase.

With the aim of exploring the effect of these inclusions on the magnetic properties, in this work we study the amorphization of Fe-Nb-B alloy using two different types of commercial boron, as well as a boron free Fe-Nb alloy for comparison.

## II. EXPERIMENTAL

Two Fe<sub>75</sub>Nb<sub>10</sub>B<sub>15</sub> alloys were prepared using Fe and Nb powders (≥99% purity) and (a) commercial amorphous

boron (95%–97% purity), denoted as a-B alloy, and (b) crystalline boron (≥99% purity), denoted as c-B alloy. Fe<sub>75</sub>Nb<sub>10</sub> alloy (denoted as n-B) was also prepared for comparison. A mixture of elemental powders was used as starting material for milling in a planetary mill Fritsch Pulverisette 4 Vario, with steel balls and hardened steel vials. Experimental conditions were powder mass 30 g, ball to powder ratio 10:1, rotational speed of the main disc 350 rpm and rotational speed of the vials 700 rpm in opposite direction. Hysteresis loops at room temperature were recorded using a Lakeshore 7407 vibrating sample magnetometer (VSM) with a maximum applied field of  $H = 1.5$  T. Saturation magnetization,  $M_s$ , was obtained from the extrapolation of high field magnetization curves,  $M(H)$ , to zero field. Powder particles were glued to prevent particle rotation.<sup>6</sup> X-ray diffraction (XRD) was performed using Cu-K $\alpha$  radiation. In the XRD patterns, amorphous phase can be recognized by a broad halo due to the short range order existing in this phase. These patterns were fitted in the angular range  $25 < 2\theta < 60$  using a Lorentzian profile to represent the crystalline phase and a Gaussian profile to the amorphous halo.<sup>7</sup> Therefore, the crystalline fraction,  $X_C$ , was estimated as the area ratio of the (110) diffraction maximum of the  $\alpha$ -Fe type phase and the sum of this area and the corresponding one to the amorphous halo. Error of  $X_C$  decreases as  $X_C$  decreases from ~15% ( $X_C \sim 0.8$ ) to ~1% ( $X_C < 0.1$ ). Microstrains and crystal sizes were estimated with Topas program<sup>8</sup> using Pawley method.<sup>9</sup> Errors in microstrains and crystal size are always below 7% and 12%, respectively.

## III. RESULTS AND DISCUSSION

The boron containing alloys developed an amorphous phase during milling, with a larger fraction for the a-B alloy. In the case of n-B alloy, a bcc-Fe(Nb) supersaturated solid solution was observed as the final microstructure. Figure 1 shows XRD patterns for samples milled 40 h. A detailed study of the microstructure evolution with the milling time can be found elsewhere.<sup>10</sup>

<sup>a)</sup>Author to whom correspondence should be addressed. Electronic mail: [jhonipus@us.es](mailto:jhonipus@us.es). Fax: +34-95 461 20 97.

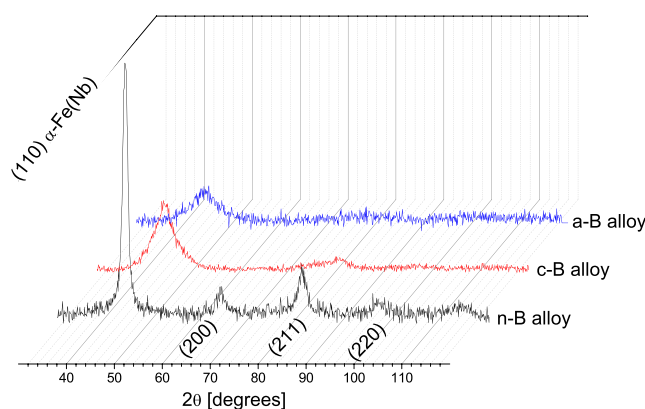


FIG. 1. XRD patterns of the three studied alloys after 40 h milling showing the characteristic halo of the amorphous phase only for B containing alloys.

Figure 2 shows room temperature saturation magnetization,  $M_S$ , and coercivity,  $H_C$ , as a function of milling time. An initial decrease in  $M_S$  can be seen for all alloys. Whereas n-B alloy shows a minimum at 4 h milling and reaches a stable value of  $143 \pm 2$  emu/g for longer milling times, B containing alloys exhibit a continuous decrease in  $M_S$  ascribed to the increase of paramagnetic amorphous phase fraction as milling progresses.

Figure 3 shows the relationship between  $M_S$  and  $X_C$  (obtained from XRD) for boron containing alloys. In the case of c-B alloy, data follows a linear trend (results from 150 rpm milling, rescaled using the equivalent milling time approach, are also included<sup>11</sup>). However, in the case of a-B alloy, two linear regions could be established, being the intercept of the linear region for high  $X_C$  far from zero. During milling, two effects take place: development of a paramagnetic amorphous phase and B enrichment of the crystalline phase. The first one causes a decrease in  $M_S$ , whereas the second one produces the opposite effect. Therefore, the

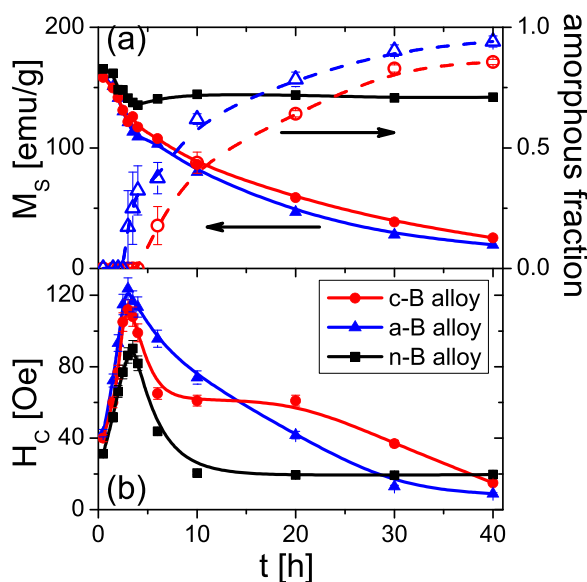


FIG. 2. (a) Saturation magnetization (solid symbols and left axis) and amorphous fraction estimated from XRD (hollow symbols and right axis) as a function of milling time. Error bars for  $M_S$  are smaller than symbol size. (b) Coercivity values as a function of milling time. Lines are guides to the eye.

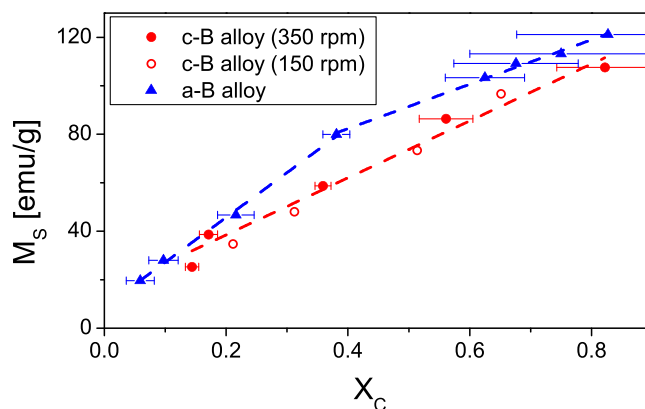


FIG. 3. Saturation magnetization as a function of the crystalline fraction estimated from XRD data. Dashed lines are linear fitting to the data. Hollow symbols correspond to c-B alloy milled at 150 rpm. Error bars for  $M_S$  are smaller than symbol size.

non-zero intercept is an artifact ascribed to a non constant value of the intrinsic magnetization of the ferromagnetic crystalline  $\alpha$ -Fe(Nb,B) phase. In fact, the commercial amorphous boron used is composed of approximately 50% of amorphous phase and 50% of crystalline one.<sup>10</sup> Crystalline boron is hardly incorporated into the matrix, remaining as inclusions even after long milling times.<sup>4,5</sup> The incorporation of amorphous boron into both phases (amorphous and crystalline solid solution) seems to be more effective, thus a higher boron content in the  $\alpha$ -Fe(Nb,B) phase implies a higher value of  $M_S$  for the same crystalline fraction. This agrees with the experimental results shown in Fig. 3, where  $M_S$  for a-B alloy is higher than c-B for any  $X_C$  value. The linear region for low  $X_C$  (long milling times) for a-B alloy would occur once the amorphous boron is incorporated, whereas crystalline boron (remaining as inclusions) is hardly incorporated into the matrix, as it occurs in the case of c-B alloy. The rate of incorporation of B from the crystalline inclusions must be too low to significantly affect the magnetization of the crystalline solid solution.

In the case of the evolution of  $M_S$  for n-B alloy, the main feature is the minimum observed after 4 h milling (Fig. 2). This minimum agrees with a maximum of the fraction of Fe atoms with very low hyperfine field measured from Mössbauer spectrometry, which was described in terms of the ductile Nb crystals deformation and the incorporation of Nb into the matrix.<sup>10</sup>

The evolution of  $H_C$  can be explained in terms of two regimes affecting magnetic anisotropy:<sup>6</sup> for short milling times, magnetic anisotropy strongly depends on the increase of microstrains and, once microstrains are saturated, the evolution of the nanocrystalline microstructure determines the variation of magnetic anisotropy, as described by Shen *et al.*<sup>12</sup>

Figure 4(a) shows the effective anisotropy,  $K_{eff}$ , calculated as  $K_{eff} = \frac{M_S H_C}{p_c}$  (where  $p_c = 0.64$  for cubic particles<sup>13</sup>), as a function of the calculated microstrains for milling times below 4 h. The expected linear correlation can be observed for all the alloys. The extrapolated  $K_{eff}$  values to zero microstrains are between 10 and 5 times smaller than that of  $\alpha$ -Fe ( $\sim 50$  kJ/m<sup>3</sup>),<sup>14,15</sup> which implies that the reduction in  $K_{eff}$  due

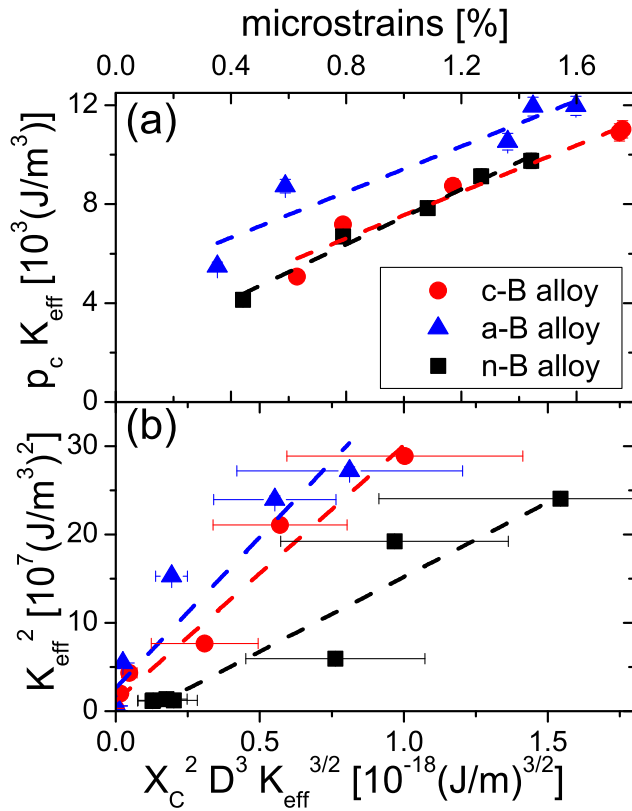


FIG. 4. Linear fitting of (a) effective anisotropy as a function of microstrains ( $t < 4$  h). Error bars for microstrains are smaller than symbol size. (b) Square effective anisotropy as a function of  $X_C^2 D^3 K_{eff}^{3/2}$  ( $t > 4$  h), as predicted by Eq. (1).

to the nanometric size of  $\alpha$ -Fe crystallites also affects the soft magnetic properties in this region.

After the saturation of microstrains, the effective anisotropy is affected by magnetoelastic and magnetocrystalline anisotropies<sup>15</sup> and according to Shen *et al.*,<sup>12</sup> it can be described as a sum of squares: long-range magnetoelastic ( $K_{\sigma,ma}$ ), averaged short-range magnetoelastic ( $\langle K_{\sigma,mi} \rangle$ ) and averaged magnetocrystalline ( $\langle K_1 \rangle$ ) anisotropies. Taking into account that the only ferromagnetic phase is the crystalline one, the expression for  $K_{eff}$  is

$$K_{eff} = \sqrt{\left(\frac{3}{2} \lambda_S \sigma_{ma}\right)^2 + \left[\left(\frac{3}{2} \lambda_S \sigma_{mi}\right)^2 + K_1^2\right] \frac{X_C^2 D^3 K_{eff}^{3/2}}{A^{3/2}}}, \quad (1)$$

where  $\lambda_S$  is the magnetostriction,  $\sigma_{ma}$  and  $\sigma_{mi}$  are the macroscopic range (corresponding to the powder particle) and microscopic range (corresponding to the crystal) of the fluctuating internal stresses, respectively,  $D$  is the average crystal size,  $X_C$  is the crystalline fraction, and  $A$  is the exchange stiffness constant. Plotting  $K_{eff}^2$  as a function of  $X_C^2 D^3 K_{eff}^{3/2}$ , a linear trend might be expected, as shown in Figure 3(b) for milling times above 4 h. From the values of

the slope and considering  $A = 10^{-11} \text{ J/m}$ , we can obtain the sum of squares of short-range and magnetocrystalline anisotropies:  $K_{\sigma,mi}^2 + K_1^2 = 67 \pm 7$ ,  $61 \pm 5$ , and  $47 \pm 5 \text{ kJ/m}^3$  for a-B, c-B, and n-B alloys, respectively. These values are of the order of the magnetocrystalline anisotropy of  $\alpha$ -Fe.

#### IV. CONCLUSIONS

Saturation magnetization and magnetic anisotropy evolutions during mechanical alloying process have been studied for three alloys: two  $\text{Fe}_{75}\text{Nb}_{10}\text{B}_{15}$  alloys prepared using crystalline and commercial amorphous boron and a third alloy without boron preserving the Fe/Nb ratio. Only the alloys with boron form an amorphous phase, which is paramagnetic at room temperature, whereas boron free alloy yields a supersaturated  $\alpha$ -Fe(Nb) solid solution as the final microstructure.

Evolution of saturation magnetization indicates that boron is more efficiently incorporated into the matrix using amorphous boron, especially for short milling times, when the intrinsic magnetization of the crystalline phase might increase as boron enters this phase.

Magnetic anisotropy evolution can be understood distinguishing by two regimes: before and after the saturation of microstrains. The first regime is governed by the progressive increase of microstrains, although a reduction of average magnetocrystalline anisotropy due to crystal sizes reduction down to nanometric scale is also inferred at this stage. The second regime is mainly governed by evolution of crystal size and amorphous fraction with a magnetic anisotropy mainly governed by magnetocrystalline contribution.

#### ACKNOWLEDGMENTS

This work was supported by the Spanish Ministry of Science and Innovation (MICINN) and EU FEDER (Project No. MAT2010-20537) and the PAI of the Regional Government of Andalucía (Project No. P10-FQM-6462). J.J.I. acknowledges a research contract from the Regional Government of Andalucía.

<sup>1</sup>M. E. McHenry *et al.*, *Prog. Mater. Sci.* **44**, 291–433 (1999).

<sup>2</sup>Y. Yoshizawa *et al.*, *J. Appl. Phys.* **64**, 6044 (1988).

<sup>3</sup>L. Schultz, *Mater. Sci. Eng.* **97**, 15–23 (1988).

<sup>4</sup>J. J. Ipus *et al.*, *Philos. Mag.* **89**, 1415–1423 (2009).

<sup>5</sup>A. H. Taghvaei *et al.*, *Mater. Chem. Phys.* **134**, 1214–1224 (2012).

<sup>6</sup>J. J. Ipus *et al.*, *J. Alloys Compd.* **509**, 1407–1410 (2011).

<sup>7</sup>R. K. Nandi and S. P. S. Gupta, *J. Appl. Crystallogr.* **11**, 6 (1978).

<sup>8</sup>Bruker AXS, Diffract Plus TOPAS version 3.0, User's Manual.

<sup>9</sup>G. S. Pawley, *J. Appl. Crystallogr.* **14**, 357 (1981).

<sup>10</sup>J. J. Ipus *et al.*, *J. Alloys Compd.* **553**, 119–124 (2013).

<sup>11</sup>J. J. Ipus *et al.*, *Intermetallics* **16**, 1073–1082 (2008).

<sup>12</sup>T. D. Shen *et al.*, *Phys. Rev. B* **72**, 014431 (2005).

<sup>13</sup>G. Herzer, *IEEE Trans. Magn.* **26**, 1397 (1990).

<sup>14</sup>R. C. O'Handley, *Modern Magnetic Materials Principles and Applications* (Wiley, New York, 2000).

<sup>15</sup>K. Suzuki and G. Herzer, *Scr. Mater.* **67**, 548–553 (2012).